Published in final edited form as:
Psychiatry Res. 2007 February 28; 154(2): 181–190. doi:10.1016/j.pscychresns.2006.08.006.

Validity of large-deformation high dimensional brain mapping of the basal ganglia in adults with Tourette syndrome

Lei Wang[a,*], **David Y. Lee**[a], **Ellen Bailey**[a], **Johanna M. Hartlein**[a], **Mohktar H. Gado**[c], **Michael I. Miller**[d], and **Kevin J. Black**[a,b,c]

[a] Department of Psychiatry, Washington University School of Medicine, St. Louis, MO, USA

[b] Department of Neurology, Washington University School of Medicine, St. Louis, MO, USA

[c] Department of Radiology, Washington University School of Medicine, St. Louis, MO, USA

[d] Center for Imaging Science, The Johns Hopkins University, Baltimore, MD, USA

Abstract

The basal ganglia and thalamus may play a critical role for behavioral inhibition mediated by prefrontal, parietal, temporal, and cingulate cortices. The cortico-basal ganglia-thalamo-cortical loop with projections from frontal cortex to striatum, then to globus pallidus or to substantia nigra pars reticulata, to thalamus and back to cortex, provides the anatomical substrate for this function. In-vivo neuroimaging studies have reported reduced volumes in the thalamus and basal ganglia in individuals with Tourette Syndrome (TS) when compared with healthy controls. However, patterns of neuroanatomical shape that may be associated with these volume differences have not yet been consistently characterized. Tools are being developed at a rapid pace within the emerging field of computational anatomy that allow for the precise analysis of neuroanatomical shape derived from magnetic resonance (MR) images, and give us the ability to characterize subtle abnormalities of brain structures that were previously undetectable. In this study, T1-weighted MR scans were collected in 15 neuroleptic-naïve adults with TS or chronic motor tics and 15 healthy, tic-free adult subjects matched for age, gender and handedness. We demonstrated the validity and reliability of large-deformation high dimensional brain mapping (HDBM-LD) as a tool to characterize the basal ganglia (caudate, globus pallidus and putamen) and thalamus. We found no significant volume or shape differences in any of the structures in this small sample of subjects.

Keywords

Shape; Reliability; Diffeomorphism

1. Introduction

Tourette syndrome (TS) is defined as a chronic idiopathic syndrome with both motor and vocal tics beginning before adulthood (American Psychiatric Association, 2000; TSCS, 1993). Tics are suppressible, stereotyped movements or vocalizations, such as blinking, sniffing, touching the ground, or tensing the abdomen. Tourette syndrome, once thought to be rare and uniformly severe, is now diagnosed reliably in more mildly affected subjects and careful epidemiological studies place its point prevalence at about 0.5% of school-age children (reviewed in (Black and Webb, 2005)). TS is highly heritable but no specific genes

*Corresponding author. Department of Psychiatry (Box 8134) Washington University School of Medicine, 660 S. Euclid Ave., St. Louis, MO 63110, USA. Tel.: +1 314 362 2417; fax: +1 314 747 2182., lei@wustl.edu (L. Wang).

have been strongly implicated in causing TS and pathophysiology is incompletely understood.

Modulation of activity in the basal ganglia and thalamus is thought to be critical for the behavioral inhibition that is exerted by the prefrontal, parietal, temporal, and cingulate cortices (Goldman-Rakic, 1987), and defects in the modulation of activity in these subcortical structures may underlie the failure to inhibit unwanted impulses in patients with TS (Mink, 2001; Peterson et al., 1998). Modulation of cortical activities by the basal ganglia and thalamus is effected through projections between the frontal cortex and the caudate nucleus, and from the caudate nucleus to the globus pallidus, substantia nigra, and thalamus. The projection from the thalamus back to the cortex completes the cortico-basal ganglia-thalamo-cortical loop (Parent and Hazrati, 1995). Although the exact physiological mechanism by which this circuitry initiates and regulates appropriate response of the motor cortex during tic suppression is unknown, sensorimotor circuits within the basal ganglia and the thalamus as well as the motor relay nuclei in the thalamus have a strong influence on such responses through reciprocal projections with the prefrontal cortex (Graybiel, 1990; Knight et al., 1995; Parent and Hazrati, 1995).

There is limited post-mortem evidence for abnormalities of brain structure in TS. As TS is (fortunately) rarely fatal, only a handful of autopsied cases have been reported. Most abnormalities were in the basal ganglia, yet this was also the region most carefully scrutinized because of *a priori* hypotheses (Swerdlow and Young, 2001). Also, new onset of tics has been noted after focal brain lesions of the prefrontal cortex, thalamus and basal ganglia. Finally, degenerative illnesses including encephalitis lethargica, Huntington disease, Wilson disease, euroacanthocytosis, and frontal lobe degenerations, have also been associated with tics or other stereotyped movements (Jankovic, 2001). Taken together, these observations provide support for the hypothesis that abnormalities of the functional interaction between the basal ganglia, thalamus and frontal cortex is involved in the development of TS (Black and Webb, 2005).

Brain structure has been examined using MRI in TS (Berthier et al., 1993; Castellanos et al., 1996; Gerard and Peterson, 2003; Peterson, 2001; Peterson et al., 1998, 2001, 2003). The results of these studies indicate that individuals with TS had smaller volumes in specific basal ganglia nuclei and the thalamus when compared with healthy controls. However, abnormalities of neuroanatomical shape that may be associated with these volume reductions have not yet been characterized. Shape abnormalities of these deep brain nuclei, if demonstrated, can become possible endophenotypes for genetic studies. They localize volume reductions to specific regions of the structure and therefore may give us additional insights into the nature of their involvement in TS and provide direction to future studies. Because neuroanatomical shapes may be influenced by patterns of neuroanatomical connections (Van Essen, 1997), metrics related to shape may be particularly sensitive to subtle disturbances in neuronal organization during development that underlie neuropsychiatric disorders such as TS.

Computational anatomy (CA) is being increasingly used to characterize abnormalities of brain structure in individuals with neuropsychiatric disorders (Ashburner et al., 2003; Thompson and Toga, 1997). It offers new approaches for precisely quantifying neuroanatomical shapes as well as volumes (Grenander and Miller, 1998) despite the variability inherent in normal anatomy (Ashburner et al., 2003; Csernansky et al., 2004b), and is a powerful approach for analyzing the detailed conformation of neuroanatomical substructures within highly complex systems. Governed by Grenander's general pattern theory (Grenander, 1993), CA represents anatomies as deformable templates, with the space of the anatomies being the set of images generated by the group of diffeomorphic (a map

between two anatomies is diffeomorphic if the map is a bijection and has a differentiable inverse) transformations acting on a neuroanatomical template, with associated probability laws that describe how they occur and how they vary. The transformations are detailed enough so that a large family of shapes can be generated with the precise topology of the template maintained. Within this framework, there exist three principal components: (i) the computation of large-deformation maps, i.e., for any given coordinate system representations of two anatomies, compute the diffeomorphic transformation from one to the other; (ii) the computation of empirical probability laws of anatomical variation between anatomies; and (iii) the construction of inferences regarding clinical categories. In this way, variabilities of brain structures can be characterized by probabilistic transformations of the neuroanatomical template as it is mapped onto target images. Every voxel in the atlas is mapped onto the targets via these transformations so that all the detailed anatomical features of the template are maintained. We call this *large-deformation high-dimensional brain mapping* (HDBM-LD).

High dimensionality and geometry-preserving properties of HDBM-LD make this method uniquely valuable for mapping complex neuroanatomies and distinguish it from lower dimensional transformations (e.g., affine or elastic). An additional virtue of the method is that it is automated, enhancing reliability and decreasing time required for analysis and reliance on expert judgment. HDBM-LD has been applied with increasing success to the problem of identifying subtle brain structure abnormalities associated with neuropsychiatric disorders (e.g., schizophrenia (Csernansky et al., 2002, 2004a; Wang et al., 2001), dementia of the Alzheimer type (Csernansky et al., 2000; Wang et al., 2003) and epilepsy (Hogan et al., 2004). The thalamus has been studied with HDBM-LD (Csernansky et al., 2004a), but the basal ganglia has not.

In the present article, we report a validation of HDBM-LD mapping of basal ganglia structures, and apply basal ganglia and thalamus HDBM-LD to analyze the shape and volume of these structures in adults with Tourette Syndrome compared to healthy controls.

2. Subjects and methods

2.1. Subjects

Fifteen adult subjects with TS (all were neuroleptic-naïve) and 15 healthy matched controls were included in the study. Each TS subject was paired with a control subject by gender, handedness (right-handed vs. non-right-handed) and age. The group characteristics are as follows: TS, m/f=10/5, mean (S.D.) age=33.4 (11.0), mean (S.D.) age of onset=6.5 (3.6), comorbid with ADHD=1, OCD=3, 13 right-handed (RH); Control, m/f=10/5, mean (S.D.) age=33.1 (11.6), 13 RH. All subjects were examined by a board-certified psychiatrist with movement disorders training. Of the 15 TS subjects, 13 met DSM-IV-TR criteria for Tourette's Disorder and 2 for Chronic Tic Disorder. The control subjects had no movement disorder. The control subjects pool was a retrospective convenience sample of subjects who had high-quality MR images as part of several different PET studies. As a consequence, diagnostic methods for comorbidity differed between groups.

2.2. Image collection and preprocessing

T1-weighted structural images were acquired on a 1.5T Siemens Sonata system and a standard head receiver coil. The main field was shimmed and the transmitter tuned before each scanning session. The anatomic image used a 3D T1-weighted sequence (MPRAGE; TR=9.7 ms, TE=4 ms, flip angle=12°, matrix=256×256, 128 partitions, field of view 160 mm, for 1×1×1.25 mm^3 voxels) (Mugler and Brookeman, 1990). Each MPRAGE acquisition requires about 6.5 min.

For image analysis, 3D reconstructions of brains were obtained using Analyze™ software (Rochester, Minnesota). MR data files were identified by number only to maintain blind conditions for image analysis. Signed 16-bit MR datasets were compressed to unsigned 8-bit MR datasets by linearly rescaling the voxel intensities, such that voxels with intensity levels at two standard deviations above the mean level in corpus callosum were mapped to 255, and voxels with intensity levels at two standard deviations below the mean in the lateral ventricles were mapped to 0. The white matter and CSF means and standard deviations were obtained by sampling voxels from these regions.

As a final step in the preprocessing of MR images, neuroanatomical landmarks were placed. In each scan, twelve global landmarks were placed at the external boundaries of the brain and at the points where the anterior and posterior commissures intersected the mid-sagittal plane (Haller et al., 1997). The placements of these global landmarks followed exactly as those described and illustrated originally in (Haller et al., 1997): at AC, PC, and points at the periphery of the cerebrum. Local landmarks were placed at select points surrounding structures of interest (see below). Initial landmark-based registration (Haller et al., 1997; Joshi et al., 1995) served to adjust the orientation and size for the head (based on global landmarks) and the basal ganglia structures (based on local landmarks), therefore provided only starting values for the HDBM-LD methods, which then proceed independent of further user input.

2.3. Neuroanatomical templates of the thalamus and basal ganglia structures

The templates for the thalamus and basal ganglia structures were generated using a high-quality T1-weighted MR sequence, averaged from seven acquisitions in another healthy comparison subject that was not otherwise included in the analysis.[1] The thalamus and basal ganglia structures in the right hemisphere were manually outlined in this MR scan by LW and MG using atlas guidelines (Mai et al., 1997) (see Fig. 1). Dr. Gado is a neuroradiologist with extensive neuroanatomical research experience.

The thalamus, caudate nucleus, putamen, globus pallidus and nucleus accumbens have been selected for study, because the literature suggests that neuroanatomical features of these structures are abnormal in TS and are a likely anatomical substrate for key functional deficits (e.g., tic suppression). Rules used for the anatomical localization of these brain structures are described in detail below.

2.3.1. Thalamus—The first anterior slice of the thalamus is taken to be immediately posterior to the descending column of the fornix, although there may be some thalamus in the last slice where fornix is seen. In the medio-lateral dimension, the thalamus extends from the third ventricle or the midline to the internal capsule. Dorsally, it is bounded by the lateral ventricle and, dorsolaterally, by the caudate nucleus. The inferior edge of the thalamus is taken to be a horizontal line extending from the ventromedial part of the internal capsule to the bulge in the third ventricle (the hypothalamic sulcus).

This boundary separates the thalamus from the hypothalamus. In its posterior half, the thalamus enlarges laterally, as the internal capsule also moves laterally. The inferior edge of the thalamus extends across the internal capsule ventrolaterally to include the lateral geniculate nucleus, which can be distinguished lateral and posterior to the internal capsule, and superior and medial to the hippocampus. The medial geniculate nucleus is inserted between the posterior part of the lateral geniculate and the rest of the thalamus, dorsal to

[1]The anatomical template (averaged scan) was provided to us by Surgical Navigation Technologies LC (Boulder, CO) along with the segmentations and surfaces for the thalamus and the basal ganglia. We made modifications to these segmentations according to the rules explained below.

cerebral peduncle. At this posterior level, where the posterior commissure becomes distinguishable, the thalamus is pushed laterally by the pretectal nuclei, and then by the periaque-ductal gray and the superior colliculus, and no longer extends to the edge of the third ventricle.

2.3.2. Caudate nucleus—The caudate nucleus is a large C-shaped deep gray matter mass located medial to the internal capsule and related throughout its length to the surface of the lateral ventricle. It has an expanded rostral component (head) that bulges into the lateral wall of the frontal horn of the lateral ventricle, and tapers to form the tail located along the lateral wall of the lateral ventricle, and then becomes further attenuated as it courses along the roof of the temporal horn of the lateral ventricle. The tail terminates at the amygdaloid nucleus. The head forms a convexity into the anterior horn of the lateral ventricle. The tail forms the lateral wall of the body of the lateral ventricle and occupies a position in the roof of the inferior (i.e., temporal) horn of the lateral ventricle. In essence, the caudate nucleus follows the curvature of the lateral ventricle.

2.3.3. Putamen—The putamen is a wedge-shaped deep gray matter mass located lateral to the caudate nucleus, with the base (larger end) of the wedge anteriorly and its tapering end posterior. It is incompletely separated from the caudate by the anterior limb of the internal capsule. In their most rostral extents, the caudate nucleus and the putamen are continuous around the anterior limb of the internal capsule, and ventrally are poorly differentiated from the nucleus accumbens.

2.3.4. Globus pallidus—The globus pallidus is a wedge-shaped deep gray matter mass located between the putamen and posterior limb of the internal capsule. The base (larger end) of the wedge lies against the medial aspect of the putamen and the tapering end lies against the internal capsule. The putamen and the globus pallidus are separated by a thin lamina of myelinated fibers called the external medullary lamina. A similar lamina (internal medullary lamina) divides the GP into a lateral or external division (GPe) and a medial or internal (GPi) division. The globus pallidus is traversed by numerous myelinated fibers, which provide its characteristic pale appearance in T1-weighted MR images.

2.3.5. Nucleus accumbens—The nucleus accumbens is situated adjacent to the medial and ventral parts of the caudate/putamen. The nucleus accumbens is the gray matter mass connecting the inferior aspects of the anterior ends of the putamen and the head of the caudate nucleus.

The putamen and the globus pallidus together constitute the main bulk of the lentiform nucleus (excluding the claustrum). The anterior part of the putamen and the caudate head are interconnected by gray matter bands (or striae), giving rise to the term corpus striatum. The caudate nucleus and the lentiform nucleus constitute the basal ganglia. The nucleus accumbens borders the inferior component of the caudate head, which is continuous laterally with the inferior aspect of the anterior end of the putamen.

Corresponding template structures in the left hemisphere were then generated by reflecting the right templates across the midsagittal line. The most anterior boundary of the caudate nucleus and the most posterior boundary of the thalamus were identified by landmarks and a line connecting these points created an anterior/posterior axis. The region between the two points was then divided into five equally distanced slices along this axis, and in each slice, five landmarks surrounding the structures of interest were placed at predetermined places. See Fig. 2 for an illustration of the landmark placements.

2.4. Large-Deformation High-Dimensional Brain Mapping (HDBM-LD)

Our structural analysis is based on Grenander's general pattern theory (Grenander, 1993) and represents the brain structures via templates, and their variabilities via diffeomorphic transformations (a diffeomorphism is a differentiable map which has a differentiable inverse) applied to the templates (Christensen et al., 1993, 1994, 1995, Joshi et al., 1995; Miller et al., 1993). The template-target transformations are diffeomorphisms constrained by laws of continuum mechanics while allowing all data points independent freedom to match, so that the geometric properties of neuroanatomical substructures are preserved (e.g. unbroken surfaces) and their details are maintained. We call this method "large-deformation high-dimensional brain mapping (HDBM-LD)." When the boundaries of template brain structures are carried along with the transformations, the volume and shape of the same brain structures in the target scans can be quantified. HDBM-LD of the template MR scan occurred in a two-step process (Miller et al., 1997). First, it was coarsely aligned to each target scan using the previously placed landmarks, and then the diffeomorphic transformation was applied. The right-hemisphere template basal ganglia and thalamus were mapped onto the right and left hemispheres of the target scans this way. The accuracy and reliability of this process were assessed by comparing the error between expert raters and HDBM-LD mappings in 10 randomly selected individuals (five from each group).

As a covariate in the comparison analysis, total cerebral volumes (excluding the brainstem and cerebellum) were derived using a landmark-based elastic transformation of the template scan. The cerebral brain has been previously outlined manually by two of the authors (LW, MHG) in the template scan (Csernansky et al., 2000). The template scan was globally registered with the MR image of each target using a landmark-based transformation with the global landmarks, followed by an elastic transformation (with eight basis vectors having 2187 basis coefficients) (Miller et al., 1997), which matched the templates for the cerebral brain onto the target scans.

2.5. Brain structure volume and shape analyses

To quantitate brain structure volume and shape, we first superimposed a triangulated graph of points onto the gray matter of each template structure within the atlas MR scan to form a surface. Each surface was then carried along as the atlas was transformed onto the target MR scans. When the transformations were completed, surfaces were generated for all selected brain structures in all of the target scans (Csernansky et al., 2004b; Joshi et al., 1997). Vector fields were obtained by computing the displacement vectors between these surfaces and their corresponding surfaces in the template.

Brain structure volume was determined by calculating the volume enclosed by the transformation-derived surfaces. Composite surfaces for the overall subject pool and composite surfaces representing each clinical group were produced by averaging vector fields across appropriate subject groups then applying the averaged vector fields to the template surface. Volume analysis for each structure was performed by repeated measures ANOVA in a mixed model, with group as main effect and hemisphere (i.e, left and right) as repeated factors. Total cerebral brain volume and age were used as covariates. Hemisphere effect and group by hemisphere interaction would measure the degree of volumetric asymmetry and group differences in volumetric asymmetry.

Brain structure shape was measured based on the pooled covariance of the inter-subject deformation vector fields derived from the HDBM-LD transformations. Singular value decomposition (SVD) of this covariance yielded eigenvalues and a complete orthonormal set of eigenvectors that represent the shape variation for the population under study. Coefficients (i.e., eigenscores) associated with these eigenvalues and eigenvectors were

calculated for each subject and for each structure in each hemisphere (Csernansky et al., 2004b). Eigenscores based on the first 5–10 eigenvectors which explained at least 75% of the total variance were then used in a multivariate ANOVA to test for group effect.

3. Results

3.1. Validation of HDBM-LD

Ten scans were randomly selected (five from each group). Two raters manually delineated the caudate nucleus, putamen, globus pallidus and the nucleus accumbens in each scan according to the anatomical rules (above). The structures generated via HDBM-LD were compared with the average of the manual delineations. In the same ten scans, a second set of mapped structures was also generated by placing a second set of landmarks and applying HDBM-LD based on the new landmarks. The following comparisons were made: 1) the two sets of mapped structures, to assess repeatability of HDBM-LD; 2) the two sets of manual delineations, to assess inter-rater reliability of the "gold standard;" and 3) the mapped structures versus the average of manual delineations to assess the reliability of validity of HDBM-LD as compared to the "gold standard." For each of these comparisons, the following assessments of mismatch were made: volume ICC, L_1 error and surface-to-surface distance.

3.1.1. Volume ICC—Volume inter-rater correlation coefficients (ICC's) are shown in Table 1 for each of the anatomical regions.

3.1.2. L_1 error—To quantify the accuracy of the automatic segmentations, we have compared them to reference segmentations generated by trained individuals. For measuring the accuracy, we use the L_1 error between positive summable functions (Joshi et al., 1999; Ratnanather et al., 2004). Specifically, let $\mathcal{M}$ be a reference manual segmentation of the image such that each of the m-compartments is labeled with a tag from 1 to m. For example, for three-compartment segmentations (m=3), label 1 represents CSF, 2 represents gray matter, 3 represents white matter; and 0 represents regions of the volume which are not segmented, for instance, the background. Let $\mathcal{A}$ be an m-compartment automated segmentation with the same labeling scheme as the manual segmentation. Let $p^M(h_n|I_n)$ be the a posteriori probability of labeling h_n at voxel n for the manual segmentation. Generally, this will have a value of either 1 or 0. For example, a voxel labeled gray matter by the manual segmentation will have a probability of 1 for the m=2 compartment, and probability of 0 for the m=1 and m=3 compartments. Let $p^A(h_n|I_n)$ be the a posteriori probability of labeling h_n at the same voxel for the automated segmentation. The L_1 tissue classification error between the two segmentations is

$$L_1=\frac{1}{2N}\sum_{n=1}^{N}\sum_{i=1}^{m}|p^A(h_n=H_i|I_n)-p^M(h_n=H_i|I_n)|$$

In the case of perfectly overlapping labeling of voxels, L_1 =0. In reality, L_1 is a measure of the cost of mislabeling the voxels with respect to the reference manual segmentation.

3.1.3. Surface-to-surface distance—Another way to measure surface mismatch is to compute a distribution of point-wise errors between two surfaces. Let $v_i^{\mathcal{A}}$ be the ith vertex on the automatically generated surface $\mathcal{A}$, and let $d(v_i^{\mathcal{A}})=\min_{u^{\mathcal{M}}\in\mathcal{M}}\left\|v_i^{\mathcal{A}}-v^{\mathcal{M}}\right\|$ be the set distance function defining the minimum distance between $v_i^{\mathcal{A}}$ and the manually generated

surface $\mathcal{M}$. Then the automatic-vs-manual surface mismatch for each subject can be represented by the average of $d(v_i^{\mathcal{A}})$ over all vertices. The mean surface distances are summarized in Table 1.

3.1.4. Summary of validation—With the exception of nucleus accumbens, mapping of the basal ganglia structures showed high repeatability (first row in Table 1) of HDBM-LD, where volume ICC is high (above 90% for all structures) and at the same time both L_1 errors and surface distance are low. The volume ICC is comparable with those obtained by other groups using two sets of hand tracings (for example, see (Peterson et al., 2003)).

The automated-vs-manual comparison (second row in Table 1) showed comparable reliability as in, for example, (Magnotta et al., 1999), who reported auto-vs-manual volume ICC of 0.86 for the right caudate and 0.71 for the right putamen. With the exception of nucleus accumbens, the L_1 errors were comparable to previously published agreements on the hippocampus (Csernansky et al., 2000;Haller et al., 1997) and the thalamus (Csernansky et al., 2004a) using HDBM-LD.

For all comparisons, the surface-to-surface distances were comparable across all the basal ganglia structures, indicating similar degree of mismatches. The disparity between the distance measure and the L_1 error could be explained by the fact that L_1 error is a relative quantity (relative to the size of the structure) whereas the distance measures the absolute difference between the mapped boundaries of the structure. Therefore structures of much smaller size (such as the nucleus accumbens) will have larger L_1 errors but similar surface distances. However, since the L_1 error measures the mismatch relative to the structural size, when it is large, we conclude that reliability cannot be demonstrated; such is the case of the nucleus accumbens.

The mapping of the thalamus has been validated previously (Csernansky et al., 2004a), with an average L_1 error of 0.082 (S.D.=0.008) between HDBM-LD mapping and expert rater manual segmentation.

3.2. Group comparisons of volumes

Repeated-measures ANOVA of each structure showed no significant group effect. Structural volumes and ANOVA statistics are shown in Table 2. Further, we found no hemisphere effect or group by hemisphere interactions for any of the structures.

3.3. Shape comparisons

Shape deformation of the adult TS subjects as compared with the controls are shown in Fig. 3. MANOVA (using the first ten eigenscores) of each structure in each hemisphere showed no significant group effect (see Table 3).

4. Discussion

We have demonstrated the validity and repeatability of mapping the basal ganglia structures, except for nucleus accumbens, using HDBM-LD to a relevant clinical population, i.e. adults with Tourette Syndrome. For the caudate nucleus, putamen and globus pallidus, the errors between segmentations generated by the HDBM-LD mapping and human raters (validity), as well as errors between repeated HDBM-LD mappings (repeatability) are 1) better or comparable with the errors between human raters, 2) comparable with errors obtained on other brain structures of similar size using similar approaches. We also examined the surface displacement errors between mapping methods and observed that, compared with the other basal structures, the nucleus accumbens had much higher L_1 errors due to its smaller

structural size even though the absolute surface mismatch was comparable. We concluded that surface-displacement errors provided alternative reliablity estimates for delineation of small brain structures such as the nucleus accumbens, either by manual outlining or the mapping algorithm.

Several prior studies have assessed volume of thalamus and basal ganglia in TS (reviewed in (Peterson et al., 2001, 2003). The largest such study used manual segmentation of MR images to identify striatum and globus pallidus in 154 TS subjects and 130 tic-free control subjects. About 40% in each group were adults (Peterson et al., 2003). The most significant abnormality was reduced caudate volume in adults and children with TS (by 4–5%). The regional volumes were highly correlated with whole brain volume. In our study, ANOVA on the volumes of the basal ganglia structures showed no group differences, nor any group×structure interaction. However, the current sample size may have offered too little statistical power (see Table 2 for effect size). Also, our study included only neuroleptic-naïve adult TS subjects. Neuroleptic drugs increase striatal volume, including in TS (Peterson et al., 2003). However, in the Peterson et al. (2003) study, TS vs. control findings were similar in the 127 TS subjects who were not taking dopamine antagonists when studied, and only 10 of these had taken them for a limited time at least 3 years prior. Finally, our results raise the question of whether the thalamus and the basal ganglia structures in these neuroleptic-naive adult subjects with TS are similar to normal adult subjects. Conceivably, our careful matching of each subject for age provided a more appropriate control for age than does linear covariation of regional volume with age.

Additional limitations of this study include the following. First, the methods described here depend heavily on the quality of the MR image data. As better resolution scanning sequences become available, their use very likely will increase the precision of our assessments. Also, non-uniformities in the MR image data due to poor calibration and field inhomogeneities may result in mismatches of gray and white matter, because our current tools are not driven solely by information about geometric structure. We have worked hard to control these sources of error using conventional strategies. In addition, we have recently begun to develop transformation tools that are driven solely by geometry and will therefore be invariant to non-uniformities in the MR images. Second, our methods are not entirely automatic, and the expertise of the expert neuroanatomist continues to play a key role. The expert creates landmark information in the MR scans, and these landmark may bias the initial landmark-driven transformations. However, it has been shown (see Section 3 and (Haller et al., 1997)) that our method is superior in reliability to the results obtained from manual outlining.

In summary, we demonstrated feasibility, accuracy and high reliability of HDBM-LD of basal ganglia in adults. Initial application of this method to a neuroleptic-naïve adult TS sample found no significant difference in shape or volume of thalamus, striatum or globus pallidus compared to carefully matched controls.

Acknowledgments

The authors acknowledge PHS support: R01-MH56584, the Conte Center for the Neuroscience of Mental Disorders at Washington University School of Medicine (P20-MH071616), P41-RR15241, and a grant from the Tourette Syndrome Association. The authors thank Joel S. Perlmutter, M.D., for providing some of the MR scans.

References

American Psychiatric Association. Diagnostic and Statistical Manual of Mental Disorders. 4. APA; Washington, DC: 2000.

Ashburner J, Csernansky JG, Davatzikos C, Fox NC, Frisoni GB, Thompson PM. Computer-assisted imaging to assess brain structure in healthy and diseased brains. Lancet Neurology 2003;2:79–88. [PubMed: 12849264]

Berthier ML, Bayes A, Tolosa ES. Magnetic resonance imaging in patients with concurrent Tourette's disorder and Asperger's syndrome. Journal of the American Academy of Child Adolescent Psychiatry 1993;32:633–639.

Black, KJ.; Webb, H. Tourette syndrome and other tic disorders. eMedicine Journal. 2005. http://www.emedicine.com/neuro/topic664.htm

Castellanos FX, Giedd JN, Hamburger SD, Marsh WL, Rapoport JL. Brain morphometry in Tourette's syndrome: the influence of comorbid attention-deficit/hyperactivity disorder. Neurology 1996;47:1581–1583. [PubMed: 8960751]

Christensen, GE.; Rabbitt, RD.; Miller, MI. In: Prince, J.; Runolfsson, T., editors. A deformable neuroanatomy textbook based on viscous fluid mechanics; 27th Annual Conference on Information Sciences and Systems; Baltimore, Maryland: Johns Hopkins University; 1993. p. 211-216.

Christensen GE, Rabbitt RD, Miller MI. 3D brain mapping using a deformable neuroanatomy. Physics in Medicine and Biology 1994;39:609–618. [PubMed: 15551602]

Christensen, GE.; Rabbitt, RD.; Miller, MI.; Joshi, SC.; Grenander, U.; Coogan, TA. Topological properties of smooth anatomical maps. In: Bizais, Braillot; Paola, D., editors. Information Processing in Medical Imaging. Vol. 3. Kluwer Academic Publishers; Boston: 1995. p. 101-112.

Csernansky JG, Wang L, Joshi S, Miller GP, Gado M, Kido D, McKeel D, Morris JC, Miller MI. Early DAT is distinguished from aging by high-dimensional mapping of the hippocampus. Dementia of the Alzheimer type. Neurology 2000a;55:1636–1643. [PubMed: 11113216]

Csernansky JG, Wang L, Jones D, Rastogi-Cruz D, Posener JA, Heydebrand G, Miller JP, Miller MI. Hippocampal deformities in schizophrenia characterized by high dimensional brain mapping. American Journal of Psychiatry 2002;159:2000–2006. [PubMed: 12450948]

Csernansky JG, Schindler MK, Splinter NK, Wang L, Gado M, Selemon LD, Rastogi-Cruz D, Posener JA, Thompson PA, Miller MI. Abnormalities of thalamic volume and shape in schizophrenia. American Journal of Psychiatry 2004a;161:896–902. [PubMed: 15121656]

Csernansky JG, Wang L, Joshi SC, Ratnanather JT, Miller MI. Computational anatomy and neuropsychiatric disease: probabilistic assessment of variation and statistical inference of group difference, hemispheric asymmetry, and time-dependent change. Neuroimage 2004b;23 (Suppl 1):S56–S68. [PubMed: 15501101]

Gerard E, Peterson BS. Developmental processes and brain imaging studies in Tourette syndrome. Journal of Psychosomatic Research 2003;55:13–22. [PubMed: 12842227]

Goldman-Rakic, P. Circuitry of primate prefrontal cortex and regulation of behavior by representation memory. In: Mountcastle, V.; Plum, F.; Geiger, S., editors. Handbook of Physiology: the Nervous System. American Physiological Socity; Bethesda, MD: 1987. p. 254-373.

Graybiel AM. Neurotransmitters and neuromodulators in the basal ganglia. Trends in Neurosciences 1990;13:244–254. [PubMed: 1695398]

Grenander, U. General Pattern Theory: a Mathematical Study of Regular Structures. Oxford University Press; Oxford: 1993.

Grenander U, Miller MI. Computational anatomy: an emerging discipline. Quarterly of Applied Mathematics 1998;56:617–694.

Haller JW, Banerjee A, Christensen GE, Gado M, Joshi S, Miller MI, Sheline Y, Vannier MW, Csernansky JG. Three-dimensional hippocampal MR morphometry with high-dimensional transformation of a neuroanatomic atlas. Radiology 1997;202:504–510. [PubMed: 9015081]

Hogan RE, Wang L, Bertrand ME. MRI-based high-dimensional hippocampal mapping in mesial temporal lobe epilepsy. Brain 2004;127:1731–1740. [PubMed: 15231583]

Jankovic J. Differential diagnosis and etiology of tics. Advances in Neurology 2001;85:15–29. [PubMed: 11530424]

Joshi, S.; Miller, MI.; Christensen, GE.; Coogan, TA.; Grenander, U. The generalized dirichlet problem for mapping brain manifolds. Int'l Symp on Optical Science, Engineering, and Instrumentation; 1995.

Joshi S, Miller MI, Grenander U. On the geometry and shape of brain sub-manifolds. International Journal of Pattern Recognition and Artificial Intelligence (Special Issue). 1997

Joshi M, Cui J, Doolittle K, Joshi S, Van Essen D, Wang L, Miller MI. Brain segmentation and the generation of cortical surfaces. Neuroimage 1999;9:461–476. [PubMed: 10329286]

Knight RT, Grabowecky MF, Scabini D. Role of human prefrontal cortex in attention control. Advances in Neurology 1995;66:21–34. discussion 34–6. [PubMed: 7771302]

Magnotta VA, Heckel D, Andreasen NC, Cizadlo T, Corson PW, Ehrhardt JC, Yuh WT. Measurement of brain structures with artificial neural networks: two-and three-dimensional applications. Radiology 1999;211:781–790. [PubMed: 10352607]

Mai, JK.; Assheuer, J.; Paxinos, G. Atlas of the Human Brain. Academic Press; San Diego: 1997.

Miller MI, Christensen GE, Amit Y, Grenander U. Mathematical textbook of deformable neuroanatomies. Proceedings of the National Academy of Sciences of the United States of America 1993;90:11944–11948. [PubMed: 8265653]

Miller MI, Banerjee A, Christensen GE, Joshi S, Khaneja N, Grenander U, Matejic L. Statistical methods in computational anatomy. Statistical Methods in Medical Research 1997;6:267–299. [PubMed: 9339500]

Mink JW. Basal ganglia dysfunction in Tourette's syndrome: a new hypothesis. Pediatric Neurology 2001;25:190–198. [PubMed: 11587872]

Mugler JP III, Brookeman JR. Three-dimensional magnetization-prepared rapid gradient-echo imaging (3D MP RAGE). Magnetic Resonance in Medicine 1990;15:152–157. [PubMed: 2374495]

Parent A, Hazrati LN. Functional anatomy of the basal ganglia. I. The cortico-basal ganglia-thalamo-cortical loop. Brain Research. Brain Research Reviews 1995;20:91–127. [PubMed: 7711769]

Peterson BS. Neuroimaging studies of Tourette syndrome: a decade of progress. Advances in Neurology 2001;85:179–196. [PubMed: 11530427]

Peterson BS, Skudlarski P, Anderson AW, Zhang H, Gatenby JC, Lacadie CM, Leckman JF, Gore JC. A functional magnetic resonance imaging study of tic suppression in Tourette syndrome. Archives of General Psychiatry 1998;55:326–333. [PubMed: 9554428]

Peterson BS, Staib L, Scahill L, Zhang H, Anderson C, Leckman JF, Cohen DJ, Gore JC, Albert J, Webster R. Regional brain and ventricular volumes in Tourette syndrome. Archives of General Psychiatry 2001;58:427–440. [PubMed: 11343521]

Peterson BS, Thomas P, Kane MJ, Scahill L, Zhang H, Bronen R, King RA, Leckman JF, Staib L. Basal ganglia volumes in patients with Gilles de la Tourette syndrome. Archives of General Psychiatry 2003;60:415–424. [PubMed: 12695320]

Ratnanather JT, Wang L, Nebel MB. Validation of semiautomated methods for quantifying cingulate cortical metrics in schizophrenia. Psychiatry Research 2004;132:53–68. [PubMed: 15546703]

Swerdlow NR, Young AB. Neuropathology in Tourette syndrome: an update. Advances in Neurology 2001;85:151–161. [PubMed: 11530425]

Thompson P, Toga A. Detection, visualization and animation of abnormal anatomic structure with a deformable probabilistic brain atlas based on random vector field transformations. Medical Image Analysis 1997;1:271–294. [PubMed: 9873911]

TSCS. Definitions and classification of tic disorders. The Tourette Syndrome Classification Study Group. Archives of Neurology 1993;50:1013–1016. [PubMed: 8215958]

Van Essen DC, Drury HA. Structural and functional analyses of human cerebral cortex using a surface-based atlas. Journal of Neuroscience 1997;17:7079–7102. [PubMed: 9278543]

Wang L, Joshi SC, Miller MI, Csernansky JG. Statistical analysis of hippocampal asymmetry in schizophrenia. Neuroimage 2001;14:531–545. [PubMed: 11506528]

Wang L, Swank JS, Glick IE, Gado MH, Miller MI, Morris JC, Csernansky JG. Changes in hippocampal volume and shape across time distinguish dementia of the Alzheimer type from healthy aging. Neuroimage 2003;20:667–682. [PubMed: 14568443]

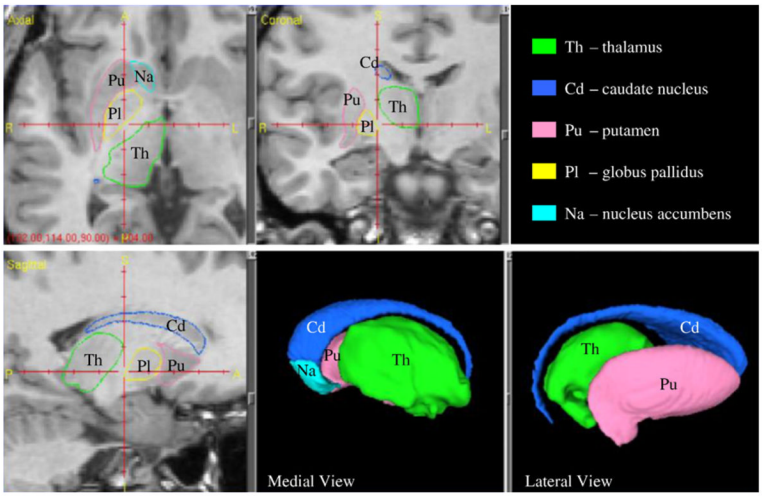

Fig. 1.

The template surfaces of the basal ganglia structures and thalamus embedded in the template MR scan. The thalamus, caudate nucleus, putamen, globus pallidus and nucleus accumbens were manually segmented in the template MR scan. Shown here are the triangulated surfaces superimposed on each segmentation and the cross-section outlines in the template MR scan.

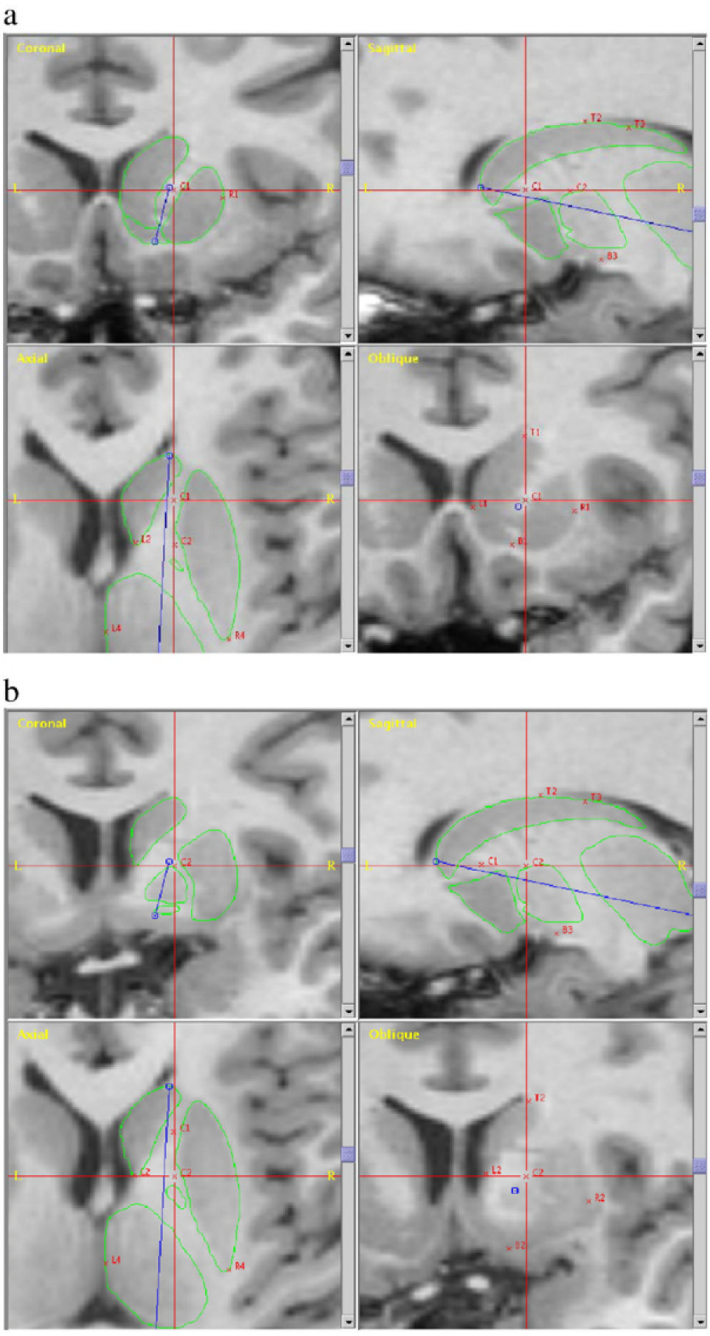

Fig. 2.

Landmarks for mapping of the basal ganglia structures and thalamus. The most anterior boundary of the caudate nucleus and the most posterior boundary of the thalamus were identified by landmarks and a line (blue) connecting these points created an anterior/posterior axis. The region between the two points was then divided into five equally distanced slices along this axis and in each slice five landmarks surrounding the structures of interest were placed at predetermined places. Panel a shows the first slice, and panel b shows the second slice. (For interpretation of the references to colour in this figure legend, the reader is referred to the web version of this article.)

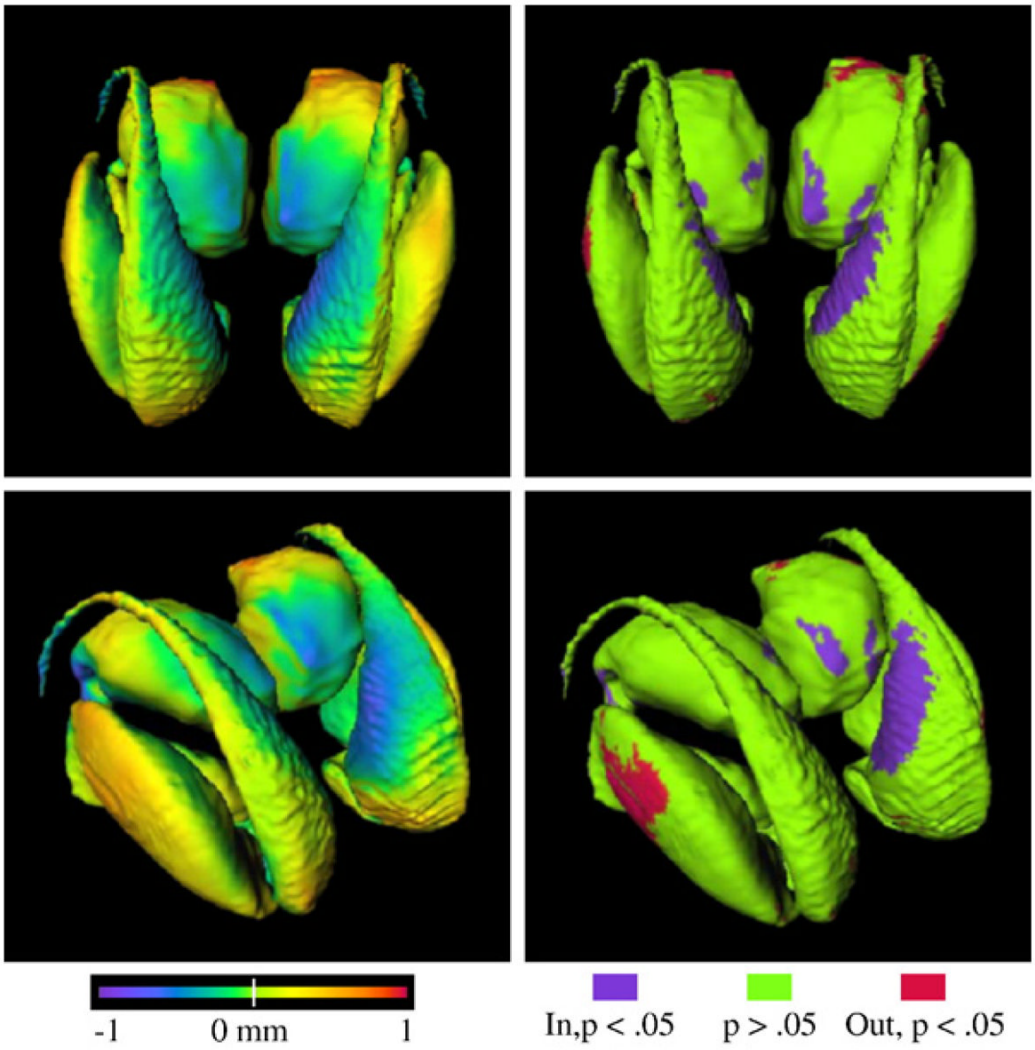

Fig. 3.

Surface deformations of adult TS subjects compared with healthy controls. Left column: surface-normal component maps, magnitude and direction of deformations are displayed as color on the mean control surfaces, with cooler colors indicating inward deformations and warmer colors indicating outward deformations. Right column: statistical significance of the deformations, via Wilcoxon's signed rank test, inward in purple ($P<0.05$), outward in red ($P<0.05$), and non-significant deformations ($P>0.05$), are shown in green. Top row: view from above. Second row: the surfaces are shown from a perspective slightly above and to the right of a midline plane, showing the top side of the structures. We note that immediately medial to the medial wall of the caudate nucleus and the anterior wall of the thalamus is the lateral ventricle. The blue colors here together with the red colors at the anterior wall of the caudate, the lateral wall of the putamen and the posterior wall of the thalamus suggest an outward movement of these structures. (For interpretation of the references to colour in this figure legend, the reader is referred to the web version of this article.)

Table 1

Validation of HDBM-LD mapping versus manual segmentation in the basal ganglia structures in 10 randomly selected individuals (five from each group)

Comparison	Caudate, R			Putamen, R			Globus pallidus, R			Nucleus accumbens		
	Vol ICC	Mean (S.D.) L_1error	Mean (S.D.) surface error (voxel)	Vol ICC	Mean (S.D.) L_1 error	Mean (S.D.) surface error voxel)	Vol ICC	Mean (S.D.) L_1 error	Mean (S.D.) surface error (voxel)	Vol ICC	Mean (S.D.) L_1 error	Mean (S.D.) surface error (voxel)
Auto 1 vs Auto 2	0.94	.079 (.048)	0.25 (0.13)	0.93	0.081 (.054)	0.29 (0.11)	0.95	0.12 (.085)	0.32 (0.13)	0.94	0.19 (0.13)	0.37 (0.16)
Auto 1 vs Average of Man	0.70	0.15 (0.03)	0.46 (0.25)	0.85	0.15 (0.02)	0.53 (0.36)	0.67	0.19 (0.02)	0.55 (0.37)	0.79	0.29 (0.04)	0.48 (0.33)
Man 1 vs Man 2	0.91	0.15 (0.07)	0.47 (0.34)	0.77	0.17 (0.03)	0.51 (0.43)	0.65	0.33 (0.07)	0.64 (0.45)	0.76	0.33 (0.05)	0.63 (0.39)

Mean (S.D.) L_1 errors and volume inter-rater correlation coefficients (ICC) between different measurements are shown here. In the first row, the comparison is made between the two sets of HDBM-LD mappings, which use two different sets of landmarks (repeatability of HDBM-LD). In the second row, the comparison is made between HDBM-LD mapping and the average of two sets of manual segmentations (validity). In the last row, the comparison is made between the two sets of manual segmentations (repeatability of raters).

Table 2

Volumes of the thalamus and basal ganglia structures and between-group comparisons

Mean (std) mm^3		**Caudate**		**Putamen**		**Globus pallidus**		**Nucleus accumbens**		**Thalamus**	
Group		**L**	**R**	**L**	**R**	**L**	**R**	**L**	**R**	**L**	**R**
TS (*n*=15)		3391 (439)	3467 (480)	4885 (627)	4763 (582)	1717 (210)	1662 (195)	456 (74)	438 (57)	7346 (883)	7263 (672)
Control (*n*=15)		3389 (258)	3411 (283)	4710 (354)	4558 (404)	1700 (133)	1601 (147)	439 (57)	426 (56)	7096 (463)	7252 (613)
Effect size (TSNCtrl) Cohen's d		0.01	0.14	0.28	0.41	0.10	0.35	0.25	0.21	0.35	0.02
ANOVA statistics	*F*	2.8		0.14		0.58		0.05		1.2	
	df	1,26		1,26		1,26		1,26		1,26	
	P	0.11		0.71		0.45		0.87		0.29	

Repeated-measures ANOVA of each structure showed no significant group effect. Further, we found no hemisphere effect or group by hemisphere interactions for any of the structures.

Table 3

Shape comparison of the thalamus and basal ganglia structures

Mean (std) mm^3		**Caudate**		**Putamen**		**Globus pallidus**		**Nucleus accumbens**		**Thalamus**	
TS vs. control		**L**	**R**	**L**	**R**	**L**	**R**	**L**	**R**	**L**	**R**
Variance accounted for (first 10 principal components)		91.6%	92.8%	92.6%	91.0%	96.7%	95.9%	98.8%	98.9%	92.2%	92.7%
ANOVA statistics	*F*	1.2	0.77	1.1	0.67	1.2	0.77	1.1	0.41	1.8	0.98
	df	10,19	10,19	10,19	10,19	10,19	10,19	10,19	10,19	10,19	10,19
	P	0.37	0.65	0.40	0.74	0.37	0.65	0.42	0.93	0.12	0.49